Ab initio Sternheimer-GW method for quasiparticle calculations using plane waves

Henry Lambert and Feliciano Giustino*
Department of Materials, University of Oxford, Parks Road, Oxford OX1 3PH, United Kingdom
(Received 21 May 2013; published 8 August 2013)

We report on the extension and implementation of the Sternheimer-GW method introduced by Giustino *et al.* [Phys. Rev. B **81**, 115105 (2010)] to the case of first-principles pseudopotential calculations based on a plane-waves basis. The Sternheimer-GW method consists of calculating the GW self-energy operator without resorting to the standard expansion over unoccupied Kohn-Sham electronic states. The Green's function is calculated by solving linear systems for frequencies along the real axis. The screened Coulomb interaction is calculated for frequencies along the imaginary axis by using the Sternheimer equation. Analytic continuation to the real axis is performed using Padé approximants. The generalized plasmon-pole approximation is avoided by performing explicit calculations at multiple frequencies using Frommer's multishift solver. We demonstrate our methodology by reporting tests on common insulators and semiconductors, including Si, diamond, LiCl, and SiC. Our calculated quasiparticle energies are in agreement with the results of fully converged calculations based on the sum-over-states approach. As the Sternheimer-GW method yields the complete self-energy $\Sigma(\mathbf{r},\mathbf{r}',\omega)$ and not only its expectation values on Kohn-Sham states, this work opens the way to nonperturbative GW calculations and to direct calculations of spectral functions for angle-resolved photoemission spectroscopy. As an example of the capabilities of the method we calculate the G_0W_0 spectral functions of silicon and diamond.

DOI: 10.1103/PhysRevB.88.075117 PACS number(s): 71.15.Qe

I. INTRODUCTION

Quasiparticle GW calculations represent nowadays an established theoretical and computational framework for studying electronic excitations.[1–4] Excitation energies calculated using the GW method are generally in good agreement with experiment in many cases, from bulk solids[3] to surfaces and interfaces,[5–7] defects,[8] and molecules.[9] Recent advances in this area include the move beyond many-body perturbation theory and the use of the GW method for total energy calculations.[10–14] For a comprehensive review of the method, history, and recent developments we refer the reader to Refs. 15–18.

Despite the successes of the GW method and the growing interest in this technology, the computational workload remains considerably heavier than in ordinary density-functional theory (DFT) calculations. As a rule of thumb, while standard DFT total energy calculations scale as N^3, N being the number of atoms in the system, the scaling of GW calculations is of the order of N^4.[19] An additional difficulty is that traditionally GW calculations rely on a slowly converging expansion over unoccupied Kohn-Sham states,[3] and in some cases fully converged calculations are exceedingly expensive. Lastly, there remains an unresolved issue concerning the energy dependence of the self-energy. While the original generalized plasmon-pole approximation and its subsequent improvements[3,20,21] are gradually being replaced by more recent approaches such as the contour deformation method[22,23] and the analytic continuation technique,[24–26] there is still a need for a more robust and accurate procedure. This need is especially relevant for the discussion of lifetime broadening in photoelectron spectroscopy.[7,27]

Several recent studies addressed some of these limitations, and devised procedures for calculating the screened Coulomb interaction more efficiently than in the standard approach. For instance Refs. 28 and 29 employ an optimal representation of the electronic polarizability operator, and Refs. 30–32 use an iterative diagonalization to determine the most significant eigenvectors of the dielectric matrix. Alternatively Refs. 33–36 improve on the sum-over-states approach by means of effective-energy techniques.

In a similar spirit Ref. 19 proposed a methodology for calculating the GW self-energy without the need for unoccupied electronic states. In this method both the Green's function and the screened Coulomb interaction are evaluated through the direct solution of linear-response Sternheimer's equations. In the following we will refer to the method of Ref. 19 as the "Sternheimer-GW" approach. The method of Ref. 19 draws from techniques well established in the context of density-functional perturbation theory for phonons,[37,38] and was used for calculating the dielectric matrix for the first time in Ref. 39. Earlier attempts along the same lines involved nonperturbative calculations using supercells.[40]

The main advantages of the Sternheimer-GW method are as follows. (i) It avoids from the outset the use of unoccupied Kohn-Sham states. This is important because fully converged calculations are challenging and in some cases it is difficult to reach a consensus on the "GW gap."[41–43] (ii) The numerical convergence of all the quasiparticle shifts (both band gaps and absolute corrections) is controlled by a single parameter, precisely as in standard DFT calculations. (iii) Despite the much improved accuracy, the computational workload is similar to or even smaller than that in current sum-over-states implementations.

In Ref. 19 the Sternheimer-GW approach was demonstrated using a proof-of-concept pilot implementation based on *empirical* pseudopotentials.[44] In the present work we report on the development and implementation of the Sternheimer-GW method in a fully *ab initio* pseudopotential implementation based on a plane-waves basis and exploiting the symmetry operations of the crystal space group. Related work is currently ongoing in order to extend the Sternheimer-GW method to the case of local orbital basis sets.[45,46]

In order to validate the *ab initio* Sternheimer-GW method we calculate the quasiparticle energies for a few standard semiconductors and insulators, including silicon, diamond, lithium chloride, and silicon carbide. We compare our calculations with the results of the standard sum-over-states approach and with experiment. We also present some initial results on the complete quasiparticle spectral functions of silicon and diamond, as obtained from our calculated GW self-energy.

The organization of the paper is as follows. Section II reviews the formalism introduced in Ref. 19. In particular we give an overview of the method in Sec. II A, we specialize the equations to the case of a plane-wave basis in Sec. II B, and we briefly discuss the calculation of the spectral function in Sec. II C. Section III addresses the technical aspects of our new developments. In particular we discuss how to exploit crystal symmetry operations in order to minimize the computational workload in Sec. III A. We address the frequency dependence of the screened Coulomb interaction and of the Green's function in Sec. III B. In this section we also discuss Padé approximants, frequency-dependent preconditioning, and the multishift solver. The computational details of the present *ab initio* implementation are described in Sec. III C. Section IV presents our numerical results, including validation tests for standard semiconductors and insulators (Sec. IV A) and calculations of complete spectral functions (Sec. IV B). We offer our conclusions and outlook in Sec. V.

II. FORMALISM FOR THE STERNHEIMER-GW METHOD

In this section we briefly review the general formalism for Sternheimer-GW calculations introduced in Ref. 19 and summarize the key equations for the case of a plane-wave basis. Throughout the paper we will refer to the G_0W_0 approximation for the self-energy, and we will limit the discussion to spin-unpolarized systems. Hartree atomic units will be used throughout.

A. Real-space formulation

In the GW approximation the self-energy Σ is given in terms of the Green's function G and the screened Coulomb interaction W by[3,15]

$$\Sigma(\mathbf{r},\mathbf{r}';\omega) = \frac{i}{2\pi}\int_{-\infty}^{\infty} G(\mathbf{r},\mathbf{r}';\omega+\omega')W(\mathbf{r},\mathbf{r}';\omega')e^{-i\delta\omega'}d\omega', \tag{1}$$

where $\mathbf{r}$ and $\mathbf{r}'$ are spatial coordinates, ω is the frequency/energy, and δ is a positive infinitesimal. The Green's function in this equation is conveniently written as the sum of a function G^{A} which is analytic in the upper half of the complex plane and a nonanalytic part G^{N}.[19] The explicit expressions of these functions in terms of single-particle states $\psi_n(\mathbf{r})$ with eigenvalues ε_n are

$$G^{\mathrm{A}}(\mathbf{r},\mathbf{r}';\omega) = \sum_n \frac{\psi_n(\mathbf{r})\psi_n^*(\mathbf{r}')}{\omega-\varepsilon_n+i\eta}, \tag{2}$$

where η is a positive real infinitesimal, and

$$G^{\mathrm{N}}(\mathbf{r},\mathbf{r}';\omega) = 2\pi i\sum_v \delta(\omega-\varepsilon_v)\psi_v(\mathbf{r})\psi_v^*(\mathbf{r}'). \tag{3}$$

The latter sum is restricted to occupied single-particle states ψ_v of energy ε_v, and the functions $\delta(\omega-\varepsilon_v)$ are Dirac's delta functions. The screened Coulomb interaction is formally defined by the following Dyson's equation:

$$W(\mathbf{r},\mathbf{r}';\omega) = v(\mathbf{r},\mathbf{r}') + \int d\mathbf{r}''\, W(\mathbf{r},\mathbf{r}'';\omega) \times \int d\mathbf{r}'''\, P(\mathbf{r}'',\mathbf{r}''';\omega)v(\mathbf{r}''',\mathbf{r}'), \tag{4}$$

where $v(\mathbf{r},\mathbf{r}') = 1/|\mathbf{r}-\mathbf{r}'|$ is the bare Coulomb interaction, and P is the irreducible polarizability. In the random-phase approximation the polarizability can be expressed in terms of single-particle states as follows:

$$P(\mathbf{r},\mathbf{r}';\omega) = 2\sum_{nm}\frac{f_n-f_m}{\varepsilon_n-\varepsilon_m-\omega}\psi_n(\mathbf{r})\psi_m^*(\mathbf{r})\psi_n^*(\mathbf{r}')\psi_m(\mathbf{r}'), \tag{5}$$

where f_n is 1 for occupied states and zero otherwise, and the factor of 2 accounts for the spin degeneracy.

In the standard sum-over-states approach the sums in Eqs. (2) and (5) are evaluated explicitly, and it is necessary to include many unoccupied states in order to achieve numerical convergence. This aspect is rather critical in many systems of current interest.[41–43,47–49] On the other hand the evaluation of the nonanalytic part of the Green's function in Eq. (3) does not pose any problems and will not be discussed further.

In the Sternheimer-GW approach the sum over unoccupied states is replaced by the solution of linear systems involving only the occupied states.[19,38,39] In order to proceed we rewrite the Green's function and the screened Coulomb interaction as functions of the space coordinate $\mathbf{r}'$, parametric in the variables $[\mathbf{r},\omega]$: $G(\mathbf{r},\mathbf{r}',\omega) = G_{[\mathbf{r},\omega]}(\mathbf{r}')$ and $W(\mathbf{r},\mathbf{r}',\omega) = W_{[\mathbf{r},\omega]}(\mathbf{r}')$. The analytic component of the Green's function is obtained by solving the following linear system:

$$(\hat{H}-\omega-i\eta)G^{\mathrm{A}}_{[\mathbf{r},\omega]} = -\delta_{[\mathbf{r}]}, \tag{6}$$

where $\hat{H}$ is the single-particle Hamiltonian (i.e., the Kohn-Sham Hamiltonian in what follows), and $\delta_{[\mathbf{r}]}$ is a Dirac delta function centered at the position $\mathbf{r}$. The screened Coulomb interaction is obtained by solving, for each occupied state ψ_v, the following two Sternheimer's equations corresponding to the choices of sign $\pm$:

$$(\hat{H}-\varepsilon_v\pm\omega)\Delta\psi^{\pm}_{v[\mathbf{r},\omega]} = -(1-\hat{P}_{\mathrm{occ}})\Delta V_{[\mathbf{r},\omega]}\psi_v. \tag{7}$$

Here $\hat{P}_{\mathrm{occ}}$ is the projection operator onto the manifold of occupied states, and $\Delta\psi^{\pm}_{v[\mathbf{r},\omega]}$ are the variations of the single-particle wave functions corresponding to the perturbation $\Delta V_{[\mathbf{r},\omega]}$. From these variations the change of the density matrix can be calculated as

$$\Delta n_{[\mathbf{r},\omega]} = 2\sum_v \psi_v^*(\Delta\psi^{+}_{v[\mathbf{r},\omega]}+\Delta\psi^{-}_{v[\mathbf{r},\omega]}). \tag{8}$$

There are *two possible choices* for the perturbation $\Delta V_{[\mathbf{r},\omega]}$ in Eq. (7). (i) If the perturbation is set to the bare Coulomb potential $\Delta V_{[\mathbf{r},\omega]} = v(\mathbf{r},\mathbf{r}')$, then it can be shown[19] that the variation of the density matrix yields the dielectric matrix:

$$\epsilon(\mathbf{r},\mathbf{r}',\omega) = \delta(\mathbf{r},\mathbf{r}') - \Delta n_{[\mathbf{r},\omega]}. \tag{9}$$

In order to obtain the screened Coulomb interaction this matrix needs to be inverted:

$$W(\mathbf{r},\mathbf{r}',\omega) = \int d\mathbf{r}'' v(\mathbf{r},\mathbf{r}'')\,\epsilon^{-1}(\mathbf{r}'',\mathbf{r}',\omega). \tag{10}$$

(ii) The second possibility is to set the perturbation in Eq. (7) to the screened Coulomb interaction: $\Delta V_{[\mathbf{r},\omega]} = W(\mathbf{r},\mathbf{r}',\omega)$. In this case the variation of the density yields a Hartree potential which screens the bare Coulomb interaction as follows:[19]

$$\Delta V_{[\mathbf{r},\omega]} = v(\mathbf{r},\mathbf{r}') + \int d\mathbf{r}'' \Delta n_{[\mathbf{r},\omega]}(\mathbf{r}'') v(\mathbf{r}'',\mathbf{r}'). \tag{11}$$

Since the perturbing potential now depends on the variation of the density, in this second option Eq. (7) needs to be solved self-consistently.

The choice between the self-consistent Sternheimer scheme and the non-self-consistent scheme depends on the system under consideration. The inversion of the dielectric matrix is very fast for small systems; hence in this case the non-self-consistent scheme of Eqs. (9) and (10) is advantageous. In the case of large systems where memory requirements are important, the self-consistent scheme of Eq. (11) is preferable.

B. Reciprocal-space formulation

In this section we summarize the equations for the Sternheimer-GW method within a plane-wave implementation. An alternative formulation based on local orbitals was presented in Ref. 45 and 46. The key advantages of a plane-wave basis are (i) the possibility of controlling the numerical accuracy of the calculations using a single parameter, i.e., the kinetic energy cutoff, and (ii) the availability of many established electronic structure codes based on plane waves.

The derivation of the following equations is given in Ref. 19; we here report only the key results. We denote by $\mathbf{G}$ and $\mathbf{G}'$ the reciprocal lattice vectors, $\mathbf{k}$ and $\mathbf{q}$ the Bloch wave vectors, and Ω the volume of the unit cell. We assume for ease of notation a uniform grid of $N_\mathbf{k}$ ($N_\mathbf{q}$) wave vectors in the first Brillouin zone, although this is not essential. Our convention for transforming a two-point function $F(\mathbf{r},\mathbf{r}',\omega)$ into its reciprocal-space counterpart $f_{[\mathbf{k},\mathbf{G},\omega]}(\mathbf{G}')$ is as follows:

$$F(\mathbf{r},\mathbf{r}',\omega) = \frac{1}{N_\mathbf{k}\Omega} \sum_{\mathbf{k},\mathbf{G}\mathbf{G}'} e^{-i(\mathbf{k}+\mathbf{G})\cdot\mathbf{r}} f_{[\mathbf{k},\mathbf{G},\omega]}(\mathbf{G}') e^{i(\mathbf{k}+\mathbf{G}')\cdot\mathbf{r}'}. \tag{12}$$

This convention is used for the Green's function G, the bare Coulomb interaction v, the screened Coulomb interaction W, and the self-energy Σ. The expansion of Bloch states $\psi_{n\mathbf{k}}$ is defined by

$$\psi_{n\mathbf{k}}(\mathbf{r}) = \frac{1}{\sqrt{\Omega}} \sum_{\mathbf{G}} u_{n\mathbf{k}}(\mathbf{G}) e^{i(\mathbf{k}+\mathbf{G})\cdot\mathbf{r}}, \tag{13}$$

where $u_{n\mathbf{k}}$ is the Bloch-periodic part of the wave function. The linear variation of the occupied eigenfunctions appearing in Eq. (7) has a slightly more complicated expansion:

$$\Delta\psi^{\pm}_{v\mathbf{k}[\mathbf{r},\omega]}(\mathbf{r}') = \frac{1}{N_\mathbf{q}\Omega} \sum_{\mathbf{q}\mathbf{G}\mathbf{G}'} e^{-i(\mathbf{q}+\mathbf{G})\cdot\mathbf{r}} e^{i(\mathbf{k}+\mathbf{q}+\mathbf{G}')\cdot\mathbf{r}'} \times \Delta u^{\pm}_{v\mathbf{k}[\mathbf{q},\mathbf{G},\omega]}(\mathbf{G}'). \tag{14}$$

Here the appearance of the Bloch wave vectors $\mathbf{k}$ and $\mathbf{k}+\mathbf{q}$ in the exponentials is a consequence of the conservation of crystal momentum in the Sternheimer equation.[19,38]

The counterpart of Eq. (6) for the analytic part of the Green's function in reciprocal space is

$$(\hat{H}_\mathbf{k} - \omega - i\eta) g^{\mathrm{A}}_{[\mathbf{k},\mathbf{G},\omega]}(\mathbf{G}') = -\delta_{-\mathbf{G}\mathbf{G}'}, \tag{15}$$

where $\hat{H}_\mathbf{k}$ indicates the $\mathbf{k}$-projected single-particle Hamiltonian. This equation is solved for each $\mathbf{k}$ and $\mathbf{G}$ using standard methods based on conjugate-gradient solvers. The frequency dependence is dealt with using Frommer's multishift method,[50] as described in Sec. III B, and effectively requires calculations only for one value of ω.

The reciprocal-space counterpart of Eq. (7) for the variation of the wave functions induced by the Coulomb interaction is

$$(\hat{H}_{\mathbf{k}+\mathbf{q}} - \varepsilon_{v\mathbf{k}} \pm \omega)\Delta u^{\pm}_{v\mathbf{k}[\mathbf{q},\mathbf{G},\omega]} = -\left(1 - \hat{P}^{\mathbf{k}+\mathbf{q}}_{\mathrm{occ}}\right)\Delta v_{[\mathbf{q},\mathbf{G},\omega]} u_{v\mathbf{k}}, \tag{16}$$

where $\hat{P}^{\mathbf{k}+\mathbf{q}}_{\mathrm{occ}}$ is the projector over the occupied states with Bloch wave vector $\mathbf{k}+\mathbf{q}$. This equation is solved for each $\mathbf{k}$, $\mathbf{q}$, $\mathbf{G}$, and ω using standard conjugate-gradient techniques. Since the linear operator $\hat{H}_{\mathbf{k}+\mathbf{q}} - \varepsilon_{v\mathbf{k}} \pm \omega$ becomes singular when the excitation energy ω corresponds to transitions between occupied and unoccupied states, we choose to calculate $\Delta u^{\pm}_{v\mathbf{k}[\mathbf{q},\mathbf{G},\omega]}$ along the imaginary axis, and to obtain the real-axis solutions by approximate analytic continuation or by means of the Godby-Needs plasmon-pole model. These aspects are described in Sec. III B. Once we have obtained the variations of the wave functions from Eq. (16) for every $\mathbf{k}$ vector we can construct the linear change in the density matrix. The reciprocal-space counterpart of Eq. (8) is

$$\Delta n_{[\mathbf{q},\mathbf{G},\omega]} = \frac{2}{N_\mathbf{k}} \sum_{v\mathbf{k}} u^*_{v\mathbf{k}} (\Delta u^{+}_{v\mathbf{k}[\mathbf{q},\mathbf{G},\omega]} + \Delta u^{-}_{v\mathbf{k}[\mathbf{q},\mathbf{G},\omega]}). \tag{17}$$

By using Eqs. (17) and (12) it is then straightforward to obtain the reciprocal-space version of Eqs. (9)–(11).

Summarizing this section, Eqs. (15) and (16) allow us to calculate the complete Green's function $G_\mathbf{k}(\mathbf{G},\mathbf{G}',\omega)$ and the complete screened Coulomb interaction $W_\mathbf{q}(\mathbf{G},\mathbf{G}',\omega)$ in reciprocal space. Once these quantities have been determined, it is possible to calculate the Bloch-periodic part of the GW self-energy $\Sigma_\mathbf{k}(\mathbf{r},\mathbf{r}',\omega)$ by transforming $\mathbf{G}$ and $\mathbf{G}'$ into real space and by evaluating the convolution

$$\Sigma_\mathbf{k}(\mathbf{r},\mathbf{r}',\omega) = \frac{i}{2\pi}\frac{1}{N_\mathbf{q}} \sum_{\mathbf{q}} \int d\omega' e^{-i\delta\omega'} \times G_{\mathbf{k}-\mathbf{q}}(\mathbf{r},\mathbf{r}',\omega+\omega') W_\mathbf{q}(\mathbf{r},\mathbf{r}',\omega'). \tag{18}$$

A step-by-step derivation of the equations presented in this section, and their relation with the standard sum-over-states approach, can be found in Ref. 19.

C. Spectral function

Since in the Sternheimer-GW approach we calculate the complete self-energy $\Sigma(\mathbf{r},\mathbf{r}',\omega)$, it is possible to investigate not only the usual quasiparticle corrections, but also the *quasiparticle spectral function*. The possibility of calculating complete spectral functions is especially important for interpreting angle-resolved photoemission (ARPES) experiments.[51,52]

For the sake of demonstrating calculations of spectral functions we here limit ourselves to considering only the diagonal elements of the GW self-energy in the basis of Kohn-Sham orbitals: $\Delta\Sigma_{n\mathbf{k}}(\omega) = \langle u_{n\mathbf{k}}|\Sigma(\mathbf{r},\mathbf{r}',\omega) - V_{\rm xc}(\mathbf{r})\delta(\mathbf{r},\mathbf{r}')|u_{n\mathbf{k}}\rangle$, where $V_{\rm xc}$ is the DFT exchange and correlation potential. This is expected to be a fair approximation for the test cases considered here,[53,54] but for more complicated situations off-diagonal terms can be included without any computational overhead.

With this choice the spectral function is also diagonal and can be calculated as follows:

$$A_{\mathbf{k}}(\omega) = \frac{1}{\pi}\sum_n \frac{|{\rm Im}\Sigma_{n\mathbf{k}}(\omega)|}{[\omega - \epsilon_{n\mathbf{k}} - {\rm Re}\Delta\Sigma_{n\mathbf{k}}(\omega)]^2 + [{\rm Im}\Sigma_{n\mathbf{k}}(\omega)]^2}. \tag{19}$$

Two illustrative examples of spectral functions calculated using this expression will be discussed in Sec. IV B.

III. COMPUTATIONAL METHODOLOGY

In this section we discuss some aspects of our methodology which are critical for achieving competitive performance. In Sec. III A we describe the reduction of the number of wave vectors $\mathbf{k}$ and $\mathbf{q}$, and reciprocal lattice vectors $\mathbf{G}$ by use of crystal symmetry operations. In Sec. III B we describe our strategy for handling the frequency dependence, and in particular the speedup achieved by using Frommer's multishift linear solver. At the end of this section we provide technical details on the implementation and on the calculations described in Sec. IV.

A. Use of crystal symmetry operations

The use of crystal symmetry operations in the context of GW calculations based on the sum-over-states approach has been discussed in Refs. 53 and 55. In this section we discuss how to minimize the computational workload of Sternheimer-GW calculations by exploiting crystal symmetry.

With reference to Sec. II B it is possible to reduce the number of $\mathbf{k}$, $\mathbf{q}$, and $\mathbf{G}$ vectors in four places: Eq. (16) needs to be solved only for inequivalent $\mathbf{G}$ vectors and $\mathbf{q}$ vectors. Equation (15) needs to be solved for inequivalent $\mathbf{G}$ vectors and $\mathbf{k}$ vectors. In Eq. (17) the sum can be restricted to the irreducible part of the Brillouin zone. In Eq. (1) the convolution requires only a subset of $\mathbf{q}$ vectors. Taken together these symmetry considerations allow us to reduce the number of independent Sternheimer equations that need to be solved.

We here denote a symmetry operation of the crystal following the notation of Ref. 56:

$$\{\mathcal{S}|\mathbf{v}\}\mathbf{r} = \mathcal{S}\mathbf{r} + \mathbf{v}, \tag{20}$$

where $\mathcal{S}$ is a rotation and $\mathbf{v}$ is the (possibly) associated fractional translation. We denote by $\mathcal{G}_{\mathbf{q}}$ the small group of $\mathbf{q}$, i.e., the subset of operations which leave this wave vector unchanged modulo a reciprocal lattice vector: $\{\mathcal{S}|\mathbf{v}\}$ such that $\mathcal{S}\mathbf{q} = \mathbf{q} + \mathbf{G}$. The self-energy Σ, the Green's function G, and the screened Coulomb interaction W are all invariant under any crystal symmetry operation $\{\mathcal{S}|\mathbf{v}\}$:

$$f(\{\mathcal{S}|\mathbf{v}\}\mathbf{r},\{\mathcal{S}|\mathbf{v}\}\mathbf{r}';\omega) = f(\mathbf{r},\mathbf{r}';\omega) \quad \text{with} \quad f = \Sigma, G, W. \tag{21}$$

By applying this relation to the Fourier expansion in Eq. (12) we obtain

$$f_{[\mathbf{q},\mathbf{G},\omega]}(\mathbf{G}') = f_{[\mathcal{S}\mathbf{q},\mathcal{S}\mathbf{G},\omega]}(\mathcal{S}\mathbf{G}')e^{i(\mathbf{G}'-\mathbf{G})\cdot\mathbf{v}}. \tag{22}$$

If $\mathbf{q}$ belongs to $\mathcal{G}_{\mathbf{q}}$ then we have a recipe for generating the solution $\Delta v_{[\mathbf{q},\mathcal{S}\mathbf{G},\omega]}$ of Eq. (16) from the solution $\Delta v_{[\mathbf{q},\mathbf{G},\omega]}$ without explicitly solving the Sternheimer equation for $\mathcal{S}\mathbf{G}$:

$$\Delta v_{[\mathbf{q},\mathcal{S}\mathbf{G},\omega]}(\mathbf{G}') = e^{-i(\mathcal{S}^{-1}\mathbf{G}'-\mathbf{G})\cdot\mathbf{v}}\Delta v_{[\mathbf{q},\mathbf{G},\omega]}(\mathcal{S}^{-1}\mathbf{G}'). \tag{23}$$

This observation implies that we need to solve the Sternheimer equation only for the subset of plane waves which are irreducible with respect to the small group $\mathcal{G}(\mathbf{q})$.

Once the solution $\Delta v_{[\mathbf{q},\mathbf{G},\omega]}(\mathbf{G}')$ has been determined for every $\mathbf{G}$ and $\mathbf{G}'$ and one wave vector $\mathbf{q}$ in the Brillouin zone, we use the symmetries of the full space group of the crystal in order to generate the symmetry-equivalent solutions for all the other wave vectors belonging to the star of $\mathbf{q}$. The transformation law is again derived from Eq. (22) and reads as follows:

$$\Delta v_{[\mathcal{S}\mathbf{q},\mathbf{G},\omega]}(\mathbf{G}') = e^{-i\mathcal{S}^{-1}(\mathbf{G}'-\mathbf{G})\cdot\mathbf{v}}\Delta v_{[\mathbf{q},\mathcal{S}^{-1}\mathbf{G},\omega]}(\mathcal{S}^{-1}\mathbf{G}'). \tag{24}$$

The sum over the wave vectors $\mathbf{k}$ in Eq. (17) can be restricted to the wedge of the Brillouin zone which is irreducible with respect to $\mathcal{G}_{\mathbf{q}}$. In order to show that this is the case, we consider the simplest case of nondegenerate bands and we rewrite the Sternheimer equation (16) for the wave vector $\mathcal{S}\mathbf{k}$, with $\mathcal{S}$ belonging to $\mathcal{G}_{\mathbf{q}}$:

$$\begin{aligned}(\hat{H}_{\mathcal{S}\mathbf{k}+\mathbf{q}} - \varepsilon_{v\mathcal{S}\mathbf{k}} \pm \omega)\Delta u^{\pm}_{v\mathcal{S}\mathbf{k}[\mathbf{q},\mathbf{G},\omega]} \\ = -\big(1 - \hat{P}^{\mathcal{S}\mathbf{k}+\mathbf{q}}_{\rm occ}\big)\Delta v_{[\mathbf{q},\mathbf{G},\omega]}u_{v\mathcal{S}\mathbf{k}}.\end{aligned} \tag{25}$$

If we now observe that $\hat{H}_{\mathcal{S}\mathbf{k}+\mathbf{q}}(\mathbf{r}) = \hat{H}_{\mathbf{k}+\mathbf{q}}(\mathcal{S}^{-1}\mathbf{r})$ and $u_{v\mathcal{S}\mathbf{k}}(\mathcal{S}\mathbf{r}) = u_{v\mathbf{k}}(\mathbf{r})$ we find

$$\begin{aligned}[\hat{H}_{\mathbf{k}+\mathbf{q}}(\mathbf{r}) - \varepsilon_{v\mathbf{k}} \pm \omega]\Delta u^{\pm}_{v\mathcal{S}\mathbf{k}[\mathbf{q},\mathbf{G},\omega]}(\mathcal{S}\mathbf{r}) \\ = -\big[1 - \hat{P}^{\mathbf{k}+\mathbf{q}}_{\rm occ}(\mathbf{r})\big]\Delta v_{[\mathbf{q},\mathbf{G},\omega]}u_{v\mathbf{k}}(\mathbf{r}).\end{aligned} \tag{26}$$

In this last equation the nonlocality of the Hamiltonian and of the projector are not displayed for clarity. By comparing Eq. (26) with Eq. (16) we obtain the transformation law for the variation of the wave functions:

$$\Delta u^{\pm}_{v\mathcal{S}\mathbf{k}[\mathbf{q},\mathbf{G},\omega]}(\mathbf{r}) = \Delta u^{\pm}_{v\mathbf{k}[\mathbf{q},\mathbf{G},\omega]}(\mathcal{S}^{-1}\mathbf{r}). \tag{27}$$

This result can be employed in Eq. (17) in order to reduce the $\mathbf{k}$ vectors to the irreducible wedge of the Brillouin zone for the small group of $\mathbf{q}$. In fact, from Eq. (9) we see that the density matrix response $\Delta n_{[\mathbf{r},\omega]}(\mathbf{r}')$ inherits the symmetry properties of the screened Coulomb interaction. In addition, from Eq. (27) we know that every term $u^*_{v\mathbf{k}}\Delta u^{+}_{v\mathbf{k}[\mathbf{q},\mathbf{G},\omega]}$ appearing in Eq. (17) transforms as the square modulus of the Bloch wave function $|u_{v\mathbf{k}}|^2$. By combining these observations together we conclude that the rule for the Brillouin zone reduction is identical to the case of standard DFT calculations of the electron density, provided the symmetries are restricted to $\mathcal{G}_{\mathbf{q}}$. This is the same rule which applies to density-functional perturbation theory calculations of phonon dispersion relations.[38] Finally, in the

case of degenerate eigenvalues this procedure holds almost unchanged, and the unitary relation between the Bloch wave functions $u_{v\mathbf{k}}$ and $u_{v\mathcal{S}\mathbf{k}}$ is traced out in the calculation of the density matrix response.

In the calculation of the Green's function $g^{\mathrm{A}}_{[\mathbf{k},\mathbf{G},\omega]}(\mathbf{G}')$ via Eq. (15) we also make use of the symmetries of the entire space group of the crystal. The transformation law is most easily seen by considering the *formal* expansion of the Green's function over the entire set of single-particle states $u_{n\mathbf{k}}$:

$$G_{\mathbf{k}}(\mathbf{r},\mathbf{r}',\omega) = \sum_n \frac{u^*_{n\mathbf{k}}(\mathbf{r})u_{n\mathbf{k}}(\mathbf{r}')}{\omega - \varepsilon_{n\mathbf{k}}}. \tag{28}$$

The same transformation law for the states $u_{n\mathbf{k}}$ leading to Eq. (26) gives in this case

$$G_{\mathcal{S}\mathbf{k}}(\mathbf{G},\mathbf{G}',\omega) = G_{\mathbf{k}}(\mathcal{S}^{-1}\mathbf{G},\mathcal{S}^{-1}\mathbf{G}',\omega), \tag{29}$$

where use was made of the convention expressed by Eq. (12).

If we now restrict the symmetry operations to the small group of $\mathbf{k}$, $\mathcal{G}(\mathbf{k}) = \{\mathcal{S}|\mathcal{S}\mathbf{k} = \mathbf{k} + \mathbf{G}\}$, then the last equation can be adapted to reduce the number of explicit solutions of Eq. (15):

$$G_{\mathbf{k}}(\mathcal{S}\mathbf{G},\mathbf{G}',\omega) = G_{\mathbf{k}}(\mathbf{G},\mathcal{S}^{-1}\mathbf{G}',\omega). \tag{30}$$

Lastly, it is possible to restrict the Brillouin zone sum in Eq. (18) by using only the $\mathbf{q}$ vectors which are irreducible with respect to the symmetry operations belonging to the small group $\mathcal{G}(\mathbf{k})$. This is possible since whenever $\mathcal{S}\mathbf{k} = \mathbf{k} + \mathbf{G}$ we can replace $G_{\mathbf{k}+\mathcal{S}\mathbf{q}}W_{\mathcal{S}\mathbf{q}}$ in Eq. (18) by its symmetry-equivalent $G_{\mathcal{S}^{-1}\mathbf{k}+\mathbf{q}}W_{\mathbf{q}} = G_{\mathbf{k}+\mathbf{q}}W_{\mathbf{q}}$. As an example of the saving afforded by the use of symmetry, in a highly symmetric crystal such as the typical example of silicon, the number of evaluations of the Sternheimer equation is reduced by a factor of ∼50.

B. Frequency dependence and multishift solver

As the Green's function and the screened Coulomb interaction both depend on the frequency ω, it is in principle necessary to solve Eqs. (15) and (16) separately for every frequency. In order to avoid the singularities in G and W along the real axis, the calculations are performed using a small imaginary component (in the case of the Green's function) or directly along the imaginary axis (in the case of the screened Coulomb interaction). The presence of an imaginary term in the frequency makes it necessary to replace the standard conjugate gradients method for the solution of these linear systems by its extension to non-Hermitian operators, such as the complex biconjugate gradients method (cBiCG).[57] In this work we employed the multishift generalization of the cBiCG algorithm described in Ref. 50 and the stabilized version of cBiCG as described in Refs. 50 and 58, hereafter referred to as BiCGStab(l). This choice is only one of several possible options; for instance the use of the generalized minimal residual method would also be possible.[59]

1. Green's function

In order to solve the non-Hermitian eigenvalue problem given by Eq. (15) we used the *multishift linear system solver* introduced by Frommer.[50] The rationale for this choice is that the multishift method enables the construction of the complete spectral structure of the Green's function at the cost of one single-frequency calculation.[19] Equation (15) is a special case of the general linear system

$$(A + \omega I)x = b, \tag{31}$$

where A is a complex linear operator, b a known complex vector, I the identity matrix, and x the unknown solution vector. This system can be thought of as being obtained from the "seed" system $Ax = b$ by "shifting" the operator A by a constant ω. Frommer's method relies on the observation that the Krilov subspaces associated with the seed and the shifted systems, i.e., $\{b, Ab, A^2b, \ldots\}$ and $\{b,(A + \omega I)b,(A + \omega I)^2b, \ldots\}$, respectively, do coincide. This makes it possible to build the solution vectors for both the seed and the shifted systems by performing only once the matrix-vector operations $Ab, A^2b, A^3b, \ldots$, and by using different coefficients for the Krilov chains.[50]

Our calculation proceeds in two steps. In the first step we address the seed system and solve Eq. (15) for $\omega = 0$ using the standard cBiCG algorithm. The cBiCG algorithm iteratively generates one sequence of solution vectors x_n, two sequences r_n and $\tilde{r}_n$ of biorthogonal residuals, and two sequences p_n and $\tilde{p}_n$ of search directions. The trial solution vector is set to $x_0 = 0$ in order to generate collinear residuals for the seed and shifted systems. The initial search directions are set to $p_0 = b$ and $\tilde{p}_0 = b^\star$. The calculation of each element of the solution sequence requires the evaluation of the following coefficients:

$$\alpha_n = \langle \tilde{r}_n | r_n \rangle / \langle \tilde{p}_n | A p_n \rangle, \tag{32}$$

$$\beta_n = -\langle A^\dagger \tilde{p}_n | r_{n+1} \rangle / \langle \tilde{p}_n | A p_n \rangle, \tag{33}$$

where $A^\dagger$ is the Hermitian conjugate of A.[57] The evaluation of the matrix-vector products Ap_n and $A^\dagger \tilde{p}_n$ is the time-consuming part of the whole procedure. As usual the iterative solution continues until the residual $r_n = b - Ax_n$ becomes smaller than a given tolerance. At each iteration the residuals r_n and the coefficients α_n and β_n are stored for subsequent use with the shifted system.

In the second step of the procedure we address the shifted systems for each frequency ω. The sequence of residuals and the coefficients calculated for the seed system are retrieved and used to generate the corresponding quantities $r_{n,\omega}$, $\alpha_{n,\omega}$, and $\beta_{n,\omega}$ for the shifted operators $A - \omega I$. The recurrence relations for the Krilov chains of the shifted system are[50]

$$r_{n,\omega} = \frac{r_n}{\pi_{n,\omega}}, \quad \alpha_{n,\omega} = \frac{\pi_{n,\omega}}{\pi_{n+1,\omega}}\alpha_n, \quad \beta_{n,\omega} = \left(\frac{\pi_{n,\omega}}{\pi_{n+1,\omega}}\right)^2 \beta_n, \tag{34}$$

with the coefficient $\pi_{n+1,\omega}$ given by

$$\pi_{n+1,\omega} = (1 + \omega\alpha_n)\pi_{n,\omega} + \frac{\alpha_n\beta_{n-1}}{\alpha_{n-1}}(\pi_{n,\omega} - \pi_{n-1,\omega}). \tag{35}$$

Owing to these relations, in the case of the shifted systems we do not perform any matrix-vector operations. Since the application of the Hamiltonian to trial solutions is the most expensive part of the solution of Eq. (15), the use of the multishift method leads to a substantial computational saving.

This procedure is amenable to efficient parallelization. Each $\mathbf{G}$ component of the Green's function $g^{\mathrm{A}}_{[\mathbf{k},\mathbf{G},\omega]}(\mathbf{G}')$ can

be calculated on one processor independently of the other components. All the vectors $g^{\mathrm{A}}_{[\mathbf{k},\mathbf{G},\omega]}$ are then collected in one place before proceeding to the evaluation of the self-energy.

For systems larger than those considered in this study, and for systems that require very high kinetic energy cutoffs, it may become necessary to use preconditioning schemes. While it should be possible to adapt polynomial preconditioners designed for Krilov multishift solvers,[60] we did not explore this direction. Instead we experimented with the calculation of the Green's function in Eq. (15) using the standard (nonmultishift) BiCGStab(l) algorithm,[58,61] combined with a slightly modified version of the Teter-Payne-Allen (TPA) preconditioner.[62]

The TPA conditioning matrix consists of a diagonal matrix whose elements are given by

$$M_{\mathbf{k}}(\mathbf{G},\mathbf{G}') = \frac{27+18x+12x^2+8x^3}{27+18x+12x^2+8x^3+16x^4}\delta_{\mathbf{G},\mathbf{G}'}, \qquad (36)$$

with $x = |\mathbf{k}+\mathbf{G}|^2/2E^{\mathrm{ref}}_{\mathrm{kin}}$ and $E^{\mathrm{ref}}_{\mathrm{kin}}$ a reference kinetic energy. This matrix ensures that the high-frequency Fourier components of the Kohn-Sham Hamiltonian (dominated by the kinetic energy) are "renormalized" to $E^{\mathrm{ref}}_{\mathrm{kin}}$, and the spectrum of the conditioned system is effectively compressed.

In the case of Eq. (15) the high-frequency Fourier components of the linear operator correspond to $|\mathbf{k}+\mathbf{G}|^2-\omega$; therefore the same effect as above is obtained by using $x = (|\mathbf{k}+\mathbf{G}|^2-\omega)/2E^{\mathrm{ref}}_{\mathrm{kin}}$ instead of the original TPA prescription. This corresponds to a translation of the TPA preconditioner along the energy axis. When $x<0$ (i.e., when $|\mathbf{k}+\mathbf{G}|^2<\omega$) we set $M_{\mathbf{k}}(\mathbf{G},\mathbf{G}') = \delta_{\mathbf{G},\mathbf{G}'}$ in order to preserve the smooth behavior of the TPA conditioner at low energy.

2. *Screened Coulomb interaction*

In the present work we consider two options for calculating the screened Coulomb interaction. (i) In order to generate the quasiparticle spectral functions we need the complete spectral structure of W. In this case we perform calculations for frequencies along the imaginary axis, followed by an approximate analytic continuation to the real axis via Padé functions. (ii) In order to make the link with GW calculations based on the sum-over-states approach we use instead the Godby-Needs plasmon pole model.[20]

A handful of techniques is currently in use for describing the frequency-dependence of the GW self-energy, from contour deformation methods[22,23] to analytic continuation techniques.[26] In the present work we choose to use Padé approximants since they provide consistently improved accuracy over standard plasmon-pole approximations.[19]

Padé approximants are routinely employed in the Eliashberg theory of superconductivity in order to calculate the superconducting gap function on the real-frequency axis, starting from the values of the gap function at the imaginary Matsubara frequencies.[63–65] In the context of GW calculations the use of Padé approximants has been demonstrated in Refs. 19,23, and 25.

Given a function $f(\omega)$ whose values are known in N distinct frequencies $\omega_1,\ldots,\omega_N$, the Padé approximant of order N is defined as the rational function of order N [i.e., with numerator and denominator of order (N div 2)] which matches f at each of these frequencies, and provides the best approximation to f outside of these points. The coefficients of the polynomials are obtained by setting $f(\omega_i) = W_{\mathbf{q}}(\mathbf{G},\mathbf{G}',\omega_i)$ for $i=1,\ldots,N$ and using the recursive algorithm of Ref. 63. Here we choose all the frequencies $\omega_1,\ldots,\omega_N$ to lie on the imaginary axis.

In the present case of Sternheimer-GW calculations the use of Padé approximants with purely imaginary frequencies is especially useful since this guarantees that the worst-case scenario for the condition number of the linear system in Eq. (16) corresponds to $\omega=0$. Other choices for the frequencies $\omega_1,\ldots,\omega_N$ are certainly possible.

The Godby-Needs plasmon-pole model can be seen as a special case of Padé approximants, where the order to the rational function is set to $N=2$ (i.e. two evaluations of W are required for each set of $\mathbf{q},\mathbf{G},\mathbf{G}'$).

The choice of calculating the screened Coulomb interaction along the imaginary axis may not be optimal in those cases where the dielectric response exhibits significant structure. However, the present method is completely flexible in terms of the choice of the frequency grid. For example, it is possible to improve the quality of the Padé continuation using exact sum rules, and also use Padé frequencies along an optimized path in the complex plane. The only requirement of our approach is that the frequency is not purely real, as this would lead to a ill-conditioned linear system in Eq. (7). The present method can also be adapted easily to alternative strategies for describing the frequency dependence of the self-energy, e.g., the contour deformation technique[23] can also be employed without requiring significant changes to the formalism or the core algorithms.

As discussed in Sec. II A we consider two strategies for obtaining the screened Coulomb interaction at each frequency via Eq. (16). In one approach we solve the *non-self-consistent* Sternheimer equation, thereby obtaining $\epsilon_{\mathbf{q}}(\mathbf{G},\mathbf{G}',\omega)$. In order to compute W the dielectric matrix is subsequently inverted following the procedure of Ref. 3. The advantage of this strategy is that we make use of Frommer's *multishift* solver (Sec. III B 1) in order to evaluate the dielectric matrix for every ω at the cost of only one frequency. In the second approach we solve the *self-consistent* Sternheimer equation, thereby obtaining directly $W_{\mathbf{q}}(\mathbf{G},\mathbf{G}',\omega)$. The advantage of this second procedure is that no explicit inversion of the dielectric matrix is performed, and the memory requirements are kept at a minimum.

C. Technical details of the implementation and calculations

The *ab initio* Sternheimer-GW method was implemented by starting from the QUANTUM ESPRESSO implementation of density-functional perturbation theory (PHONON code).[66] All ground-state DFT calculations were performed using QUANTUM ESPRESSO. GW calculations based on the sum-over-states approach were performed using the SAX code,[67] which also uses Kohn-Sham wave functions and eigenvalues obtained from QUANTUM ESPRESSO. In order to ensure consistency we used identical parameters and pseudopotentials in the ground-state DFT calculations for both Sternheimer-GW and sum-over-states calculations.

DFT calculations were performed within the local density approximation (LDA).[68,69] We used Troullier-Martins norm-conserving pseudopotentials[70] with plane-wave kinetic energy

cutoffs set to 20 Ry for Si and 60 Ry for diamond, SiC, and LiCl. We used a shifted $6 \times 6 \times 6$ Monkhorst-Pack mesh[71] in order to describe the DFT electron density, as well as the screened Coulomb interaction W. The dielectric matrices were described using kinetic energy cutoffs of 10, 24, 20, and 15 Ry for silicon, diamond, silicon carbide, and lithium chloride, respectively. The exchange part of the self-energy was calculated using the same kinetic energy cutoff as for the wave functions in all cases. The singularity in the Coulomb interaction at long wavelength was removed by using the spherical truncation scheme of Ref. 72.

The evaluation of the screened Coulomb interaction along the imaginary axis was performed at frequencies equally spaced by 2 eV up to the plasmon frequency, and equally spaced by 20 eV beyond this point and up to 100 eV. This sampling was meant to capture at once the finer structure in the dielectric response at low frequency and the asymptotic behavior at high frequency. In the case of the self-consistent solution of Eq. (16) we used an adaptive threshold in order to speed up the convergence of the combined procedure consisting of cBiCG iterations and density updates.

A generalization of the modified Broyden method for charge-density mixing[73] was used in order to minimize charge fluctuations during the self-consistent calculations.[19] In order to achieve a relative numerical convergence of 10^{-6} in the L^2 norm of W we needed at most six iterations for all systems studied here. The one exception is the long-wavelength limit $\mathbf{G} = \mathbf{G}' = 0$ and $\mathbf{q} \to \mathbf{0}$, which may require up to 30 iterations. In the case of calculations using the Godby-Needs plasmon-pole model we set the imaginary frequencies to 1.2 Ry for Si and C and 1.3 Ry for SiC and LiCl.

The Green's function was calculated at frequencies slightly off the real axis. In particular we used frequencies equally spaced by 0.1 eV in the range ± 150 eV, and with an imaginary component of 0.3 eV. The calculation of the self-energy in Eq. (18) was performed numerically along the real axis, using a spacing of 0.1 eV and a broadening of 0.3 eV. The integration boundaries were set to ± 120 eV.

Since Eq. (16) needs to be solved independently for every $\mathbf{G}$, the Sternheimer-GW approach is intrinsically parallel. In our implementation each perturbation of wave vector $\mathbf{G}$ is dealt with by one processor, and the resulting W and G are collected at the end using global communications. Figure 1 illustrates the timing of the Sternheimer-GW method in our current parallel implementation. As we increase the number of processes the calculation time decreases as expected. In the current implementation we use only one level of parallelization (over the $\mathbf{G}$ vectors). As a consequence the number of processors exceeds the number of symmetry-reduced plane-wave perturbations for certain $\mathbf{q}$ points; hence increasing the number of processors does not reduce the execution time. A second level of parallelization (over $\mathbf{q}$ vectors) would be needed in order to achieve linear parallel scaling, and it is currently under development.

From Fig. 1 we see that the calculation of W is considerably more time consuming than for G. This can be understood by comparing Eqs. (16) and (15). In fact the calculation of the screened Coulomb interaction involves solutions for $\mathbf{k}$, $\mathbf{q}$, and the valence bands, while the calculation of the Green's function involves only solutions for the various $\mathbf{k}$ vectors. The evaluation of the self-energy Σ is not parallel in the current implementation and the timing for this operation is a constant in Fig. 1.

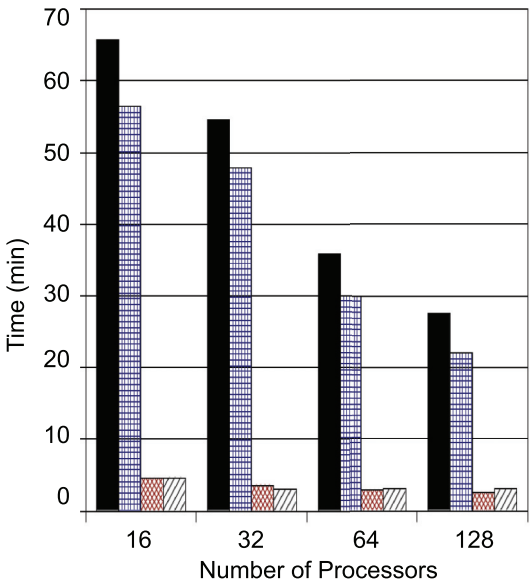

FIG. 1. (Color online) Parallel execution time for a Sternheimer-GW calculation of silicon. The time refers to a calculation of the complete self-energy $\Sigma_{\mathbf{k}}(\mathbf{G},\mathbf{G}',\omega)$ with the parameters given in Sec. III C. We report the total execution time (full black bars), the time required for calculating the screened Coulomb interaction (straight cross-hatched blue bars), the Green's function (oblique cross-hatched red bars), and the frequency convolution in Eq. (18) (oblique hatched black bars).

For the sake of clarity we point out that a sum-over-states calculation performed with a number of electronic states equal to the number of plane waves should in principle be equivalent to the Sternheimer-GW method. However, in practice performing sum-over-states calculations with the maximum possible number of unoccupied states is challenging in terms of memory requirements and diagonalization of the highest-lying states. In terms of floating-point operations, in Ref. 19 it was shown that the Sternheimer-GW method should be more efficient than the sum-over-states approach if both diagonal and off-diagonal self-energy matrix elements are to be evaluated.

IV. RESULTS

A. Quasiparticle corrections

In this section we validate our method by comparing the quasiparticle corrections of Si, C, SiC, and LiCl obtained using the Sternheimer-GW and those obtained using the sum-over-states approach. In Figs. 2 and 3 we consider the comparison between the quasiparticle corrections to the band edges in silicon and diamond, calculated by us using the Sternheimer-GW method (blue solid lines) and using the standard method as implemented in SAX (red dashed lines). In Table I we compare the quasiparticle energies of Si, C, SiC, and LiCl calculated using the Sternheimer-GW method with previous calculations and experiment. The quasiparticle corrections are defined with reference to the LDA Kohn-Sham eigenvalues using the

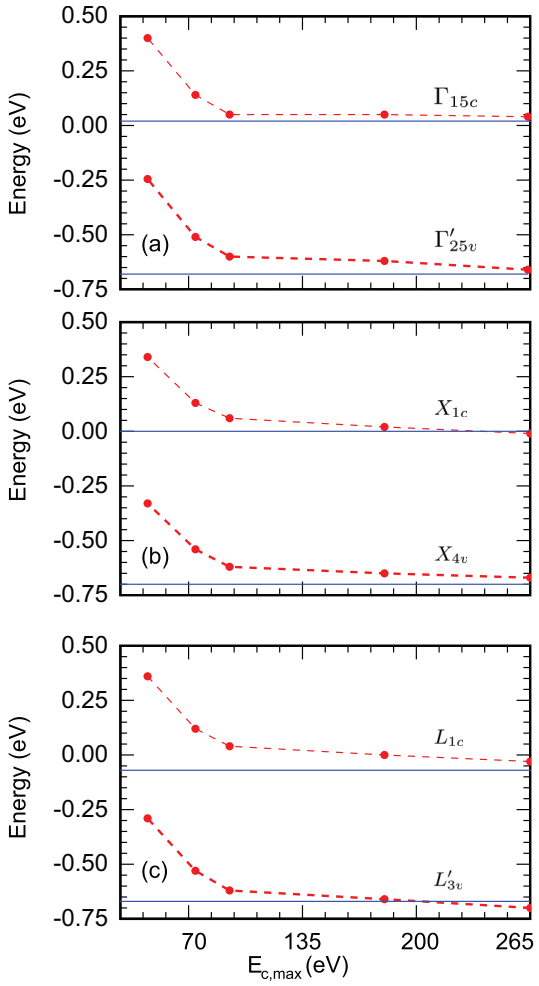

FIG. 2. (Color online) Quasiparticle corrections to the band edge states at high-symmetry points in silicon: Sternheimer-GW (solid blue line) and sum-over-states approaches as implemented in SAX (red disks and dashed line). The corrections are shown as a function of the energy of the highest unoccupied state included in the sum-over-states calculation. The zero of the energy is set to the top of the valence band. (a) Band edges at Γ, (b) band edges at X, and (c) band edges at L.

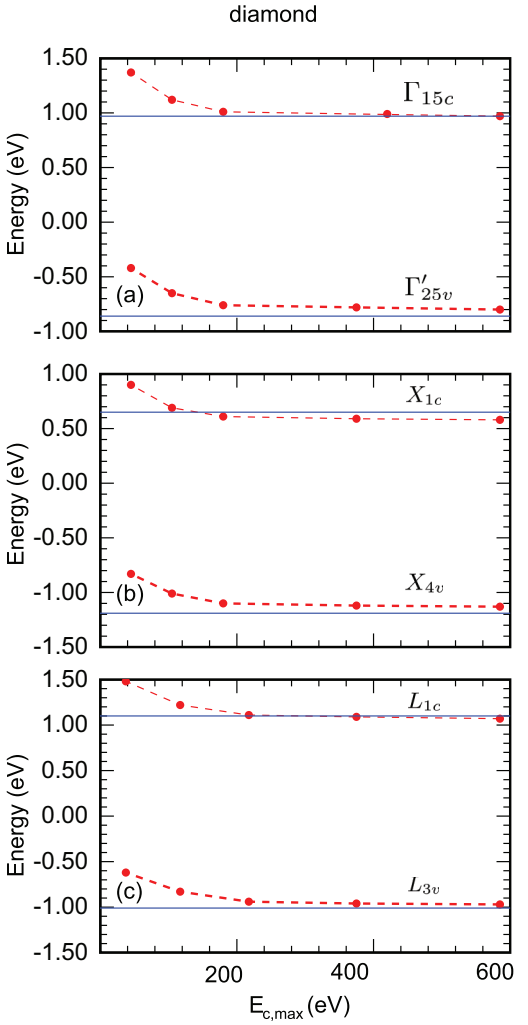

FIG. 3. (Color online) Quasiparticle corrections to the band edge states at high-symmetry points in diamond: Sternheimer-GW (solid blue line) and sum-over-states approaches as implemented in SAX (red disks and dashed line). The corrections are shown as a function of the energy of the highest unoccupied state included in the sum-over-states calculation. The zero of the energy is set to the top of the valence band. (a) Band edges at Γ, (b) band edges at X, and (c) band edges at L.

standard prescription:[3] $\Delta\varepsilon_{n\mathbf{k}} = Z_{n\mathbf{k}}\Delta\Sigma_{n\mathbf{k}}(\varepsilon_{n\mathbf{k}})$, where $Z_{n\mathbf{k}}$ is the quasiparticle renormalization of the state $u_{n\mathbf{k}}$. In all cases discussed in this section we used the Godby-Needs plasmon-pole model in order to be consistent with the sum-over-states method.

In these figures we see that our method and the standard approach yield essentially the same quasiparticle corrections, provided a large number of unoccupied states is included in the latter calculation. The convergence of *differences of quasiparticle corrections* is relatively fast within the standard approach; however, the calculation of *absolute quasiparticle energies* is considerably more challenging. In fact, fully converged sum-over-states calculations of the absolute quasiparticle energies require cutoffs comparable to that of the underlying plane-wave basis set. This result was somewhat expected since the wave-function cutoff enters the matrix elements of the polarizability in the sum-over-states approach.[3]

The fact that the Sternheimer-GW approach is able to provide absolute quasiparticle energies without the need of unoccupied states (as opposed to relative corrections) is expected to be important for the study of heterogeneous systems, such as surfaces, interfaces, and defects.

An interesting observation that we can make by inspecting Figs. 2 and 3 is that, *in fully converged calculations*, the GW correction is not concentrated on the conduction band as is generally assumed. For example in the case of silicon our calculations suggest that the quasiparticle correction is actually concentrated in the valence band (Fig. 2), while in the case of diamond the correction to the band gap is equally distributed between valence and conduction bands (Fig. 3). These findings are in line with recent calculations on oxides and semiconductors where similar trends were observed,[48,49] and suggest that some caution should be used when applying semiempirical scissor corrections.

For definiteness we now analyze in detail the calculated quasiparticle corrections to the band edge states of diamond at Γ, i.e., the Γ'_{25v} and Γ_{15c} states, shown in Fig. 3(a). This

TABLE I. Quasiparticle energies corresponding to the band edges of Si, C, SiC, and LiCl at high-symmetry points: comparison between the results of Sternheimer-GW calculations and previous work using the sum-over-states approach. The initial DFT/LDA eigenvalues are also reported for completeness. All values are in units of eV and the zero of the energy is set to the top of the valence bands in all cases. All previous calculations for silicon, diamond, and LiCl are from Ref. 23, 16, and 3, respectively.

	DFT/LDA		GW		
	Present	Previous	Present	Previous	Experiment
			Silicon		
Γ'_{25v}	0.00	0.00	0.00	0.00	0.00
Γ_{15c}	2.55	2.54	3.26	3.09	3.40[a], 3.05[b]
X_{4v}	−2.87	−2.85	−2.92	−2.90	−3.3 ± 0.2[c]
X_{1c}	0.65	0.61	1.32	1.01	1.25[b]
L_{1v}	−6.99	−6.99	−7.10	−6.97	−6.7 ± 0.2[a]
L'_{3v}	−1.21	−1.19	−1.18	−1.16	−1.2 ± 0.2[a]
L_{1c}	1.49	1.44	2.19	2.05	2.4 ± 0.15[a]
L_{3c}	3.34	3.30	4.09	3.83	4.15 ± 0.1[d]
			Diamond		
Γ'_{25v}	0.00	0.00	0.00	0.00	0.00
Γ_{15c}	5.6	5.58	7.50	7.63	7.3[a]
X_{4v}	−6.27	−6.26	−6.68	−6.69	
X_{1c}	4.65	4.63	6.12	6.30	
L_{1v}	− 13.46	−13.33	−14.18	−14.27	−12.8 ± 0.3[e]
L_{3v}	−2.82	−2.78	−2.93	−2.98	
L_{1c}	8.49	8.39	10.53	10.63	
L_{3c}	8.89	8.76	10.30	10.23	
			SiC		
Γ_{15v}	0.00	0.00	0.00	0.00	0.00
Γ_{1c}	6.34	6.25[f]	7.31	7.32[f]	7.4[g]
X_{5v}	−3.24	−3.20[h]	−3.53	−3.53[h]	
X_{1c}	1.36	1.31[h]	2.12	2.19[h]	2.39[a]
L_{3v}	−1.08	−1.06[h]	−1.07	−1.21[h]	−1.15[a]
L_{1c}	5.40	5.34[f]	6.23	6.45[f]	6.35[a]
			LiCl		
Γ_{1c}	5.90	6.00	8.80	9.10	9.4[i]
X_{4v}	−2.90	−3.00	−3.00	−3.30	
X_{5v}	−1.10	−1.10	−1.20	−1.30	
X_{1c}	7.50	7.50	10.80	10.70	

[a]Reference 74.
[b]Reference 75.
[c]Reference 76.
[d]Reference 77.
[e]Reference 78.
[f]Reference 23.
[g]Reference 79.
[h]Reference 16.
[i]Reference 80.

example is representative of all the test cases considered here. The corrections to the Γ_{15c} state calculated using the Sternheimer-GW and sum-over-states approaches are identical to within 0.01 eV. The corrections to the Γ'_{25v} state are −0.86 eV (Sternheimer-GW) and −0.80 eV (fully converged sum over states). In this case the renormalization factor (0.83) and the bare exchange contribution to the quasiparticle correction (−19.21 eV) are the same in both methods, and the small residual discrepancy of 0.06 eV comes from the correlation part of the self-energy. We assign this small discrepancy to the different strategies used to perform the frequency integral in Eq. (18), since the standard method performs an analytic integration while we use a numerical integration. At any rate these very small differences are well below the typical accuracy expected from converged GW calculations, especially if we take into account the dependence on the pseudopotentials and the DFT exchange and correlation functional.

Table I shows the quasiparticle energies of Si, C, SiC, and LiCl as obtained using the Sternheimer-GW method, compared to previously published calculations based on the sum-over-states approach, as well as experiment. In this table we set the energy zero to the top of the valence bands; therefore the values reported are truly *relative* quasiparticle corrections. The agreement of Sternheimer-GW results with previous calculations and experiment is generally very good. The small residual discrepancies of the order of 0.1 eV can tentatively be assigned to the incomplete convergence of previous calculations, although this is only a speculation.

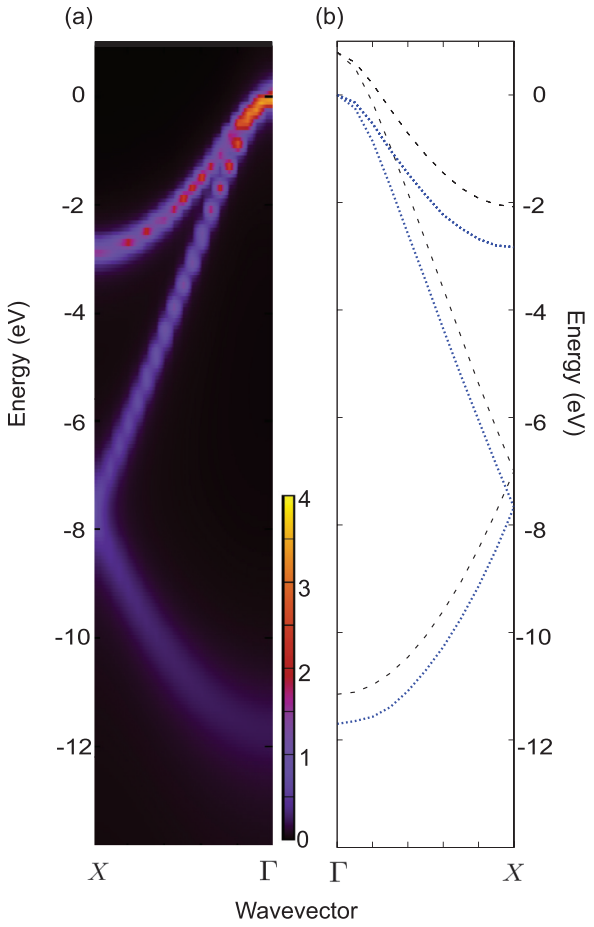

FIG. 4. (Color online) (a) Quasiparticle spectral function $A_{\mathbf{k}}(\omega)$ of silicon for $\mathbf{k}$ along Γ-X, calculated using the Sternheimer-GW method within the diagonal G_0W_0 approximation [Eq. (19)]. The "discrete" structure visible in the more dispersive band is simply a visualization artifact, resulting from our choice of computing the self-energy at 20 equally spaced $\mathbf{k}$ points. (b) DFT/LDA band structure of silicon along Γ-X (black dashed lines), and the corresponding quasiparticle band structure obtained from (a) (blue solid lines). The units of the color bar are eV^{-1}.

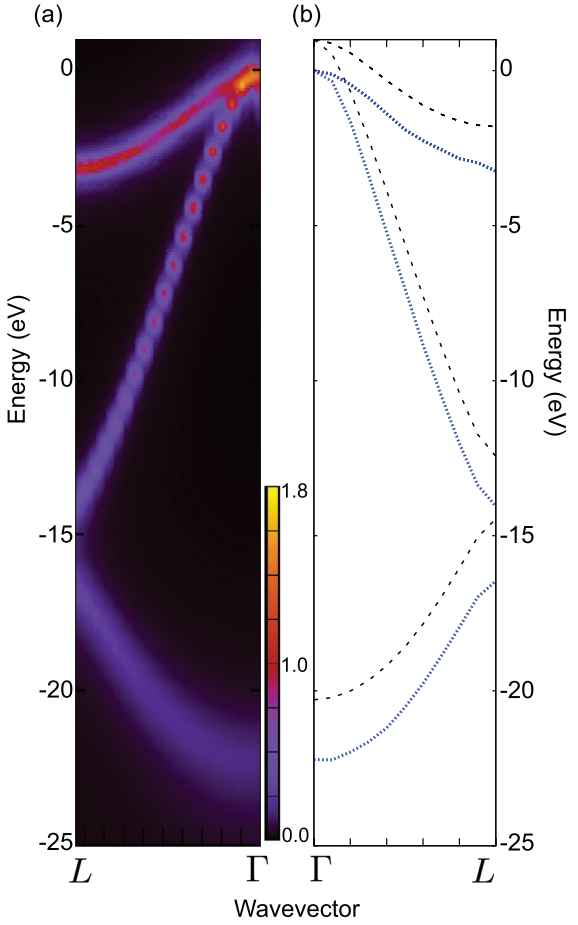

FIG. 5. (Color online) (a) Quasiparticle spectral function $A_{\mathbf{k}}(\omega)$ of diamond for $\mathbf{k}$ along Γ-L, calculated using the Sternheimer-GW method within the diagonal G_0W_0 approximation [Eq. (19)]. The "discrete" structure visible in the more dispersive band is simply a visualization artifact, resulting from our choice of computing the self-energy at 20 equally spaced $\mathbf{k}$ points. (b) DFT/LDA band structure of diamond along Γ-L (black dashed lines), and the corresponding quasiparticle band structure obtained from (a) (blue solid lines). The units of the color bar are eV^{-1}.

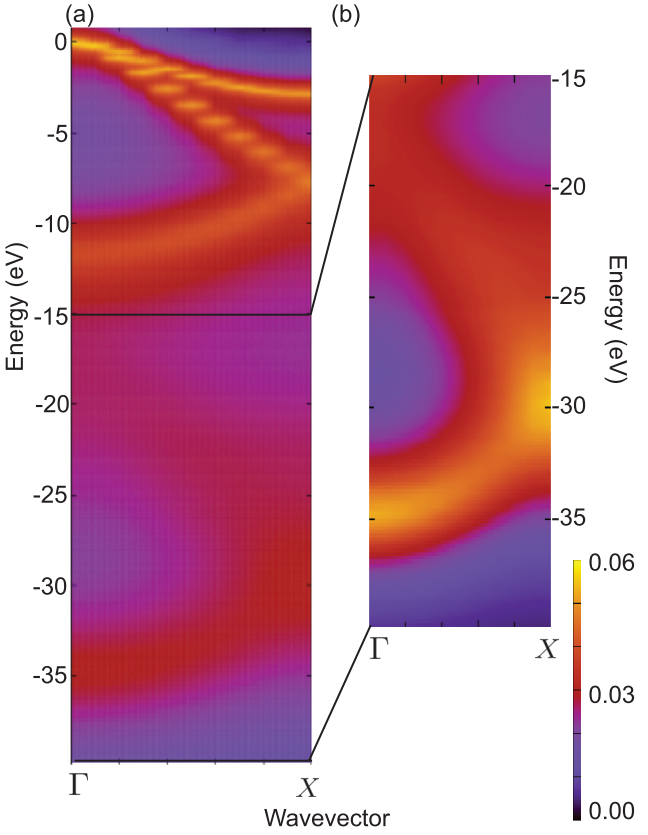

FIG. 6. (Color online) (a) Quasiparticle spectral function $A_{\mathbf{k}}(\omega)$ of silicon for $\mathbf{k}$ along Γ-X, calculated using the Sternheimer-GW method within the diagonal G_0W_0 approximation [Eq. (19)]. The energy range extends to -40 eV in order to show the plasmaron band structure. The spectral function is given in a logarithmic scale in order to enhance the plasmaron satellites. (b) Zoom on the plot in (a) around the binding energy 15–40 eV, showing the plasmaron band structure. In this case we use a linear scale with values given by the color bar. We note that the satellite energy is incorrect in the G_0W_0 approximation (Refs. 13 and 84–86). The units of the color bar are eV^{-1}.

B. Spectral functions

In this section we present examples of calculations of the quasiparticle spectral functions of silicon and diamond (Figs. 4 and 5). All the calculations were performed using Padé approximants as discussed in Sec. III B 2. Once the self-energy Σ is obtained using the Sternheimer-GW method, the evaluation of the spectral function using Eq. (19) is straightforward and is carried out as a postprocessing operation.

The availability of the spectral function makes it possible to obtain not only standard quasiparticle energies but also the intensity and widths of the quasiparticle peaks. For example, from Fig. 4 we can extract the width of the Γ_{1v} state at the bottom of the valence band of silicon. We obtain a width of 1.3 eV, corresponding to a quasiparticle lifetime of 3.2 fs. This finding is in agreement with previous G_0W_0 calculations of the spectral function of silicon.[23,81] The same analysis carried out for diamond in Fig. 5 shows that the width of the states near the valence band bottom at Γ is 1.8 eV. This finding is in line with ARPES experiments indicating a linewidth of $\sim$2 eV.[82]

We note that our calculated spectral functions carry an intrinsic linewidth of 0.3 eV. This linewidth is an artifact resulting from our choice of evaluating the Green's function at frequencies slightly off the real axis (cf. Sec. III). This artificial broadening accounts for the finite linewidths observed near the top of the valence bands in Figs. 4 and 5.

Figure 6 shows a magnification of the calculated spectral function of silicon at large binding energy (20–40 eV). In the G_0W_0 approximation the structure of the real and imaginary parts of the self-energy leads to an additional spectral feature, which was termed a "plasmaron" in Ref. 83. Interestingly such plasmaron structures exhibit energy vs wave vector dispersion relations which closely mimic the standard electron band structure in the binding energy range 0–20 eV. A more detailed analysis of these "plasmaron band structures" will be reported elsewhere. Here we limit ourselves to pointing out that the energy of such plasmarons is overestimated in G_0W_0 calculations and that more sophisticated solutions of the Hedin

equations (e.g., based on the cumulant expansion) are known to yield a series of satellites which are not captured within the G_0W_0 approximation.[13,84–86] Within this context, the current implementation of the Sternheimer-GW method carries precisely the same limitations as the G_0W_0 approximation; hence Fig. 6 is meant only to show the capabilities of the method.

We note that the G_0W_0 spectral functions obtained within the Sternheimer-GW approach could be used as a starting point for more advanced calculations of photoemission satellites.[13,86]

V. CONCLUSIONS AND OUTLOOK

In this paper we presented the implementation of the Sternheimer-GW method using first-principles pseudopotentials and a plane-waves basis. The present work extends the method of Ref. 19, where the theoretical methodology was introduced and a proof-of-concept implementation based on empirical pseudopotentials was given.

The Sternheimer-GW method presented here enables GW calculations based solely on the occupied Kohn-Sham electronic states and therefore completely eliminates the need for laborious convergence tests typical of the sum-over-states approach. As a result the Sternheimer-GW approach requires only one convergence parameter, namely, the kinetic energy cutoff of the inverse dielectric matrix.

The decoupling of the plane-wave perturbations afforded by the Sternheimer equation makes the present scheme intrinsically parallel, as we have shown in a simple test calculation on silicon.

We have demonstrated our method by considering a few standard test cases such as Si, C, SiC, and LiCl. We proved good agreement with previous GW calculations, and excellent agreement with sum-over-state calculations performed using exactly the same pseudopotentials and calculation parameters.

Our method provides the complete G_0W_0 self-energy, and therefore naturally lends itself to the study of quasiparticle spectral functions, e.g., within the context of angle-resolved photoemission experiments. We demonstrated the possibility of calculating the G_0W_0 spectral functions of silicon and diamond without any computational overheads, and we discussed additional features corresponding to plasmaron satellites. Extensions of the present method in the direction of including multiple plasmon satellites along the lines of the cumulant expansion are highly desirable.

While our method yields more information than a standard sum-over-states calculation, the calculation time is competitive owing to an extensive use of crystal symmetry operations, as well as to the adoption of a multishift iterative solver for the linear systems. Further optimization of the linear system solvers is possible and under way.

The inclusion of self-consistency in GW calculations is an important avenue for future development;[10,14] therefore we briefly comment on the possibility of extending the Sternheimer-GW method to include self-consistency. In the present formalism it should be possible to include self-consistency at the level of the quasiparticle self-consistent GW method of Ref. 10. Indeed, while this choice would result in added computational complexity, the structure of our key equations would be preserved. An additional element that could be explored is the inclusion of first-principles linewidths in in Eqs. (6) and (7). A related possibility would be to update the DFT exchange and correlation potential by using the self-energy obtained from our calculations, for example following the proposal of Ref. 87.

Since our method is based on the repeated application of the Kohn-Sham Hamiltonian to a state vector, it also represents an ideal starting point for exploring the effects of various DFT starting points in perturbative GW calculations.[48,88,89] Indeed, it should be possible to extend the present method in order to perform calculations using wave functions, eigenvalues, and screening corrections beyond the random-phase approximation, e.g., using a hybrid-functional Hamiltonian. In a time when GW calculations are rapidly becoming the standard tool for studying electronic excitations from first principles, we hope that the method presented in this work will serve as a platform for accurate, parameter-free, and reproducible quasiparticle calculations.

ACKNOWLEDGMENTS

This work was supported by the ERC under the EU FP7/ERC Grant No. 239578 and by the UK EPSRC Grant No. EP/J009857/1.

*feliciano.giustino@materials.ox.ac.uk

[1] L. Hedin, Phys. Rev. **139**, A796 (1965).
[2] G. Strinati, H. J. Mattausch, and W. Hanke, Phys. Rev. B **25**, 2867 (1982).
[3] M. S. Hybertsen and S. G. Louie, Phys. Rev. B **34**, 5390 (1986).
[4] R. W. Godby, M. Schlüter, and L. J. Sham, Phys. Rev. Lett. **56**, 2415 (1986).
[5] M. Giantomassi, M. Stankovski, R. Shaltaf, M. Grüning, F. Bruneval, P. Rinke, and G.-M. Rignanese, Phys. Status Solidi B **1**, 1 (2010).
[6] R. Shaltaf, G.-M. Rignanese, X. Gonze, F. Giustino, and A. Pasquarello, Phys. Rev. Lett. **100**, 186401 (2008).
[7] C.-H. Park, F. Giustino, C. D. Spataru, M. L. Cohen, and S. G. Louie, Nano Lett. **9**, 4234 (2009).
[8] P. Rinke, A. Janotti, M. Scheffler, and C. G. Van de Walle, Phys. Rev. Lett. **102**, 026402 (2009).
[9] C. Rostgaard, K. W. Jacobsen, and K. S. Thygesen, Phys. Rev. B **81**, 085103 (2010).
[10] M. van Schilfgaarde, T. Kotani, and S. Faleev, Phys. Rev. Lett. **96**, 226402 (2006).
[11] S. Ismail-Beigi, Phys. Rev. B **81**, 195126 (2010).
[12] M. Gatti, F. Bruneval, V. Olevano, and L. Reining, Phys. Rev. Lett. **99**, 266402 (2007).
[13] M. Guzzo, G. Lani, F. Sottile, P. Romaniello, M. Gatti, J. J. Kas, J. J. Rehr, M. G. Silly, F. Sirotti, and L. Reining, Phys. Rev. Lett. **107**, 166401 (2011).
[14] F. Caruso, P. Rinke, X. Ren, M. Scheffler, and A. Rubio, Phys. Rev. B **86**, 081102 (2012).

[15]L. Hedin and S. Lundqvist, Solid State Phys. **23**, 1 (1969).
[16]W. G. Aulbur, M. Städele, and A. Görling, Phys. Rev. B **62**, 7121 (2000).
[17]F. Aryasetiawan and O. Gunnarsson, Rep. Prog. Phys. **61**, 237 (1998).
[18]G. Onida, L. Reining, and A. Rubio, Rev. Mod. Phys. **74**, 601 (2002).
[19]F. Giustino, M. L. Cohen, and S. G. Louie, Phys. Rev. B **81**, 115105 (2010).
[20]R. W. Godby and R. J. Needs, Phys. Rev. Lett. **62**, 1169 (1989).
[21]G. E. Engel and B. Farid, Phys. Rev. B **47**, 15931 (1993).
[22]T. Kotani and M. van Schilfgaarde, Solid State Commun. **121**, 461 (2002).
[23]S. Lebègue, B. Arnaud, M. Alouani, and P. E. Bloechl, Phys. Rev. B **67**, 155208 (2003).
[24]R. Daling, W. van Haeringen, and B. Farid, Phys. Rev. B **44**, 2952 (1991).
[25]Y.-G. Jin and K. J. Chang, Phys. Rev. B **59**, 14841 (1999).
[26]H. N. Rojas, R. W. Godby, and R. J. Needs, Phys. Rev. Lett. **74**, 1827 (1995).
[27]C. D. Spataru, M. A. Cazalilla, A. Rubio, L. X. Benedict, P. M. Echenique, and S. G. Louie, Phys. Rev. Lett. **87**, 246405 (2001).
[28]P. Umari, G. Stenuit, and S. Baroni, Phys. Rev. B **79**, 201104 (2009).
[29]P. Umari, G. Stenuit, and S. Baroni, Phys. Rev. B **81**, 115104 (2010).
[30]H. F. Wilson, F. Gygi, and G. Galli, Phys. Rev. B **78**, 113303 (2008).
[31]H. F. Wilson, D. Lu, F. Gygi, and G. Galli, Phys. Rev. B **79**, 245106 (2009).
[32]T. A. Pham, H.-V. Nguyen, D. Rocca, and G. Galli, Phys. Rev. B **87**, 155148 (2013).
[33]F. Bruneval and X. Gonze, Phys. Rev. B **78**, 085125 (2008).
[34]J. A. Berger, L. Reining, and F. Sottile, Phys. Rev. B **82**, 041103 (2010).
[35]J. A. Berger, L. Reining, and F. Sottile, Phys. Rev. B **85**, 085126 (2012).
[36]J. Deslippe, G. Samsonidze, M. Jain, M. L. Cohen, and S. G. Louie, Phys. Rev. B **87**, 165124 (2013).
[37]S. Baroni, P. Giannozzi, and A. Testa, Phys. Rev. Lett. **58**, 1861 (1987).
[38]S. Baroni, S. de Gironcoli, A. Dal Corso, and P. Giannozzi, Rev. Mod. Phys. **73**, 515 (2001).
[39]L. Reining, G. Onida, and R. W. Godby, Phys. Rev. B **56**, R4301 (1997).
[40]K. Kunc and E. Tosatti, Phys. Rev. B **29**, 7045 (1984).
[41]M. Stankovski, G. Antonius, D. Waroquiers, A. Miglio, H. Dixit, K. Sankaran, M. Giantomassi, X. Gonze, M. Côté, and G.-M. Rignanese, Phys. Rev. B **84**, 241201 (2011).
[42]B.-C. Shih, Y. Xue, P. Zhang, M. L. Cohen, and S. G. Louie, Phys. Rev. Lett. **105**, 146401 (2010).
[43]C. Friedrich, M. C. Müller, and S. Blügel, Phys. Rev. B **83**, 081101 (2011).
[44]M. L. Cohen and T. K. Bergstresser, Phys. Rev. **141**, 789 (1966).
[45]H. Hübener, M. A. Pérez-Osorio, P. Ordejón, and F. Giustino, Phys. Rev. B **85**, 245125 (2012).
[46]H. Hübener, M. Pérez-Osorio, P. Ordejón, and F. Giustino, Eur. Phys. J. B **85**, 321 (2012).
[47]M. L. Tiago, S. Ismail-Beigi, and S. G. Louie, Phys. Rev. B **69**, 125212 (2004).
[48]C. E. Patrick and F. Giustino, J. Phys.: Condens. Matter **24**, 202201 (2012).
[49]R. M. Filip, E. C. Patrick, and F. Giustino, Phys. Rev. B **87**, 205125 (2013).
[50]A. Frommer, Computing **70**, 87 (2003).
[51]A. Damascelli, Z. Hussain, and Z.-X. Shen, Rev. Mod. Phys. **75**, 473 (2003).
[52]W. Bardyszewski and L. Hedin, Phys. Scr. **32**, 439 (1985).
[53]M. S. Hybertsen and S. G. Louie, Phys. Rev. B **35**, 5585 (1987).
[54]F. Bruneval, N. Vast, and L. Reining, Phys. Rev. B **74**, 045102 (2006).
[55]B. Arnaud and M. Alouani, Phys. Rev. B **62**, 4464 (2000).
[56]A. A. Maradudin and S. H. Vosko, Rev. Mod. Phys. **40**, 1 (1968).
[57]D. A. H. Jacobs, IMA J. Numer. Anal. **6**, 447 (1986).
[58]H. van der Vorst, SIAM J. Sci. Stat. Comput. **13**, 631 (1992).
[59]A. Frommer and U. Glässner, SIAM J. Sci. Comput. **19**, 15 (1998).
[60]B. Jegerlehner, arXiv:hep-lat/9612014.
[61]G. L. G. Sleijpen and D. R. Fokkema, Electron. Trans. Numer. Anal. **1**, 11 (1993).
[62]M. P. Teter, M. C. Payne, and D. C. Allan, Phys. Rev. B **40**, 12255 (1989).
[63]H. J. Vidberg and J. W. Serene, J. Low Temp. Phys. **29**, 179 (1977).
[64]K. S. D. Beach, R. J. Gooding, and F. Marsiglio, Phys. Rev. B **61**, 5147 (2000).
[65]E. R. Margine and F. Giustino, Phys. Rev. B **87**, 024505 (2013).
[66]P. Giannozzi *et al.*, J. Phys.: Condens. Matter **21**, 395502 (2009).
[67]L. Martin-Samos and G. Bussi, Comput. Phys. Commun. **180**, 1416 (2009).
[68]D. M. Ceperley and B. J. Alder, Phys. Rev. Lett. **45**, 566 (1980).
[69]J. P. Perdew and A. Zunger, Phys. Rev. B **23**, 5048 (1981).
[70]N. Troullier and J. L. Martins, Phys. Rev. B **43**, 1993 (1991).
[71]H. J. Monkhorst and J. D. Pack, Phys. Rev. B **13**, 5188 (1976).
[72]J. Spencer and A. Alavi, Phys. Rev. B **77**, 193110 (2008).
[73]D. D. Johnson, Phys. Rev. B **38**, 12807 (1988).
[74]*Numerical Data and Functional Relationships in Science and Technology*, edited by K. H. Hellwege and O. Madelung, Landolt-Börnstein, New Series, Group III, Vol. 17, pt. A and Vol. 22, pt. A (Springer, Berlin, 1982).
[75]J. E. Ortega and F. J. Himpsel, Phys. Rev. B **47**, 2130 (1993).
[76]A. L. Wachs, T. Miller, T. C. Hsieh, A. P. Shapiro, and T.-C. Chiang, Phys. Rev. B **32**, 2326 (1985).
[77]D. Straub, L. Ley, and F. J. Himpsel, Phys. Rev. Lett. **54**, 142 (1985).
[78]F. J. Himpsel, J. F. van der Veen, and D. E. Eastman, Phys. Rev. B **22**, 1967 (1980).
[79]W. R. L. Lambrecht, B. Segall, M. Yoganathan, W. Suttrop, R. P. Devaty, W. J. Choyke, J. A. Edmond, J. A. Powell, and M. Alouani, Phys. Rev. B **50**, 10722 (1994).
[80]G. Baldini and B. Bosacchi, Phys. Status Solidi B **38**, 325 (1970).
[81]B. Arnaud, S. Lebègue, and M. Alouani, Phys. Rev. B **71**, 035308 (2005).
[82]T. Yokoya, T. Nakamura, T. Matushita, T. Muro, H. Okazaki, M. Arita, K. Shimada, H. Namatame, M. Taniguchi, Y. Takano *et al.*, Sci. Technol. Adv. Mater. **7**, Suppl. 1, S12 (2006).

[83]B. Lundqvist, Phys. Kond. Mater. **6**, 193 (1967).
[84]D. C. Langreth, Phys. Rev. B **1**, 471 (1970).
[85]C. Blomberg and B. Bergersen, Can. J. Phys. **50**, 2286 (1972).
[86]J. Lischner, D. Vigil-Fowler, and S. G. Louie, Phys. Rev. Lett. **110**, 146801 (2013).
[87]R. W. Godby, M. Schlüter, and L. J. Sham, Phys. Rev. B **37**, 10159 (1988).
[88]P. Rinke, A. Qteish, J. Neugebauer, C. Freysoldt, and M. Scheffler, New J. Phys. **7**, 126 (2005).
[89]H. Jiang, R. I. Gomez-Abal, P. Rinke, and M. Scheffler, Phys. Rev. B **82**, 045108 (2010).